In situ Foaming of Porous $(La_{0.6}Sr_{0.4})_{0.98}$ $(Co_{0.2}$ $Fe_{0.8})$ $O_{3-\delta}$ (LSCF) Cathodes for Solid Oxide Fuel Cell Applications

Sodith Gandavarapu and Edward Sabolsky

US DOE-National Energy Technology Laboratory, 3610 Collins Ferry Road, P.O.Box.880, Morgantown, West Virginia, 26507

Department of Mechanical and Aerospace Engineering, West Virginia University, Morgantown, West Virginia, 26506

Katarzyna Sabolsky

Department of Mechanical and Aerospace Engineering, West Virginia University, Morgantown, West Virginia, 26506

Kirk Gerdes

US DOE-National Energy Technology Laboratory, 3610 Collins Ferry Road, P.O.Box.880, Morgantown, West Virginia, 26507

A binder system containing polyurethane precursors was used to *in situ* foam (direct foam) a $(La_{0.6}Sr_{0.4})_{0.98}$ $(Co_{0.2}$ $Fe_{0.8})$ $O_{3-\delta}$ (LSCF) composition for solid oxide fuel cell (SOFC) cathode applications. The relation between *in situ* foaming parameters on the final microstructure and electrochemical properties was characterized by microscopy and electrochemical impedance spectroscopy (EIS), respectively. The optimal porous cathode architecture was formed with a 70 vol% solids loading within a polymer precursor composition with a volume ratio of 8:4:1 (isocyanate: PEG: surfactant) in a terpineol-based ink vehicle. The resultant microstructure displayed a broad pore size distribution with highly elongated pore structure.

Introduction

The functionality of an SOFC is dependent upon the cathode to adsorb oxygen molecules, reduce oxygen, and transport oxygen ions to the bulk electrolyte for incorporation. Consequently, the SOFC cathode layer must possess adequate porosity to permit oxygen mass transport and adsorption. Cathode porosity is generated by partial densification above the fuel cell operation temperature, commonly through burnout (combustion) of a carbon fugitive material that is mixed with the cathode ink during thermal processing.[1] By specifically controlling the fugitive size and chemistry, the pore size, shape, and distribution can be designed.

An alternative to fugitive-induced porosity methods is a direct foaming method, which is a potentially quick, easily adaptable, and relatively cheap process yielding structures with a broad pore size distribution.[2] The *in situ* foaming (direct foaming) method employs a gas-evolving chemical reaction within a gel or suspension that is active during the green processing state. Depending upon the viscosity and wetting characteristics, the gas

may be trapped and/or coalesce within the suspension/gel. After thermolysis (burnout) of any binder within the suspension/gel, the trapped gas forms a network of interconnected pores within the ceramic body. The final pore size and distribution are dependent on the nucleation and growth processes of the gas phase, and the manner that the gas bubble permeates within the particulate suspension.

The adaptability of the *in situ* foaming process for forming ceramic porous structures was earlier reported by Powell *et al.*[3] In this study, a method is discussed to control porosity size and relative density of the ceramic foams by utilizing a polyurethane polymerization reactions to "blow" and "gel" ceramic suspensions. Wucherer *et al.* also used a polyurethane polymerization reaction to create $BaTiO_3$ foams through direct foaming. This work described the importance of the polymer precursor and surfactants on the resultant porous ceramic microstructure.[4] The standard polyurethane polymerization reaction consists of the use of a di-isocyanate (polymer precursor) along with a hydroxyl group (polyol). The reaction of the isocyanate component with water results in the generation of CO_2 gas and is typically termed the blowing reaction. In parallel to this reaction, the polyol reacts

*ed.sabolsky@mail.wvu.edu

with the isocyanate to form a urea bond resulting in the cross-linking of the polymer and a rigid structure. This second reaction is usually termed as the "gelation reaction." The parallel occurrence of these two reactions within a particulate suspension or sol results in the formation of a rigid foamed gel structure.

As briefly described previously, the *in situ* foaming process has extensive applications, but the process has never been extensively investigated for SOFC applications. Foamed alumina structures formed through *in situ* foaming were used as ceramic insulators in thermal management devices used in SOFC applications due to their low thermal conductivity at room temperature and 800°C.[5] The direct foaming process used in the field of solid oxide fuel cells was reported by Rainer *et al.*[2] where NiO–YSZ bulk ceramics were foamed to obtain an open-cell structure with interconnected porosity for potential anode supports. An *in situ* foaming or direct foaming process has never been demonstrated for the formation of porosity within SOFC cathode bulk material. In addition, the direct foaming of thick films on a substrate, such as cathode films onto a solid electrolyte membrane, has not been reported in literature. In this work, a polymerization reaction was chosen as the mechanism for direct foaming complex $(La_{0.6}Sr_{0.4})(Co_{0.2}Fe_{0.8})O_{3-\delta}$ (LSCF) cathode microstructures. The LSCF composition was chosen due to its high total conductivity ($\sim$ 250 S/cm at 800°C) and its mixed ionic–electronic conducting nature.[6] Mixed ionic–electronic conductors (MIECs) such as LSCF possess a high oxygen reduction capability compared with commonly used LSM/YSZ composite cathode mixtures, where the reaction is limited to the triple phase boundary (TPB) locations.[7] The goal is to develop a simple forming process that will allow for microstructural design of the cathode structure, specifically for increased TPB population, pore distribution/gradient, oxygen mass flow, and nanocatalyst incorporation.

Control of processing parameters such as precursor composition, monomer type, and solids loading of the cathode will affect the CO_2 evolution and retention within the loaded suspension, and consequently controlling the final pore architecture. Therefore, various combinations of the processing parameters of *in situ* foaming were investigated in this work allowing for optimal control of the porous structure, pore volume distribution, and porosity levels. The pore size, shape, distribution, and orientation were characterized through computational image analysis of scanning electron microscope (SEM) images. The measured microstructural parameters were contrasted to the processing variables and electrochemical testing. Finally, the *in situ* foaming process

was modified to deposit LSCF foamed thick films onto electrolyte-supported symmetrical cells for EIS testing.

Experimental

The cathode material used in this work was the $(La_{0.6}Sr_{0.4})_{0.98}(Co_{0.2}Fe_{0.8})O_{3-\delta}$ (LSCF) composition with a 2% A-site deficiency. The LSCF powder was synthesized through a solid-state process, where the raw materials of La_2O_3, $SrCO_3$, Fe_2O_3, and $CoCO_3$ (Alfa Aesar, Ward Hill, MA) were roll milled for 2 h and then attrition milled for 4 h using zirconia media. The slurry was dried and sieved through the 60 mesh (250 μm) and calcined at 900, 1000, and 1100°C for 4 h. X-ray diffraction (XRD) was performed on the calcined powder (Fig. 1), and the desired perovskite single phase (JCPDS 49-285) was displayed at 1000°C; hence, the bulk calcination was completed at this temperature. The final powder was attrition milled for 2 h in ethanol resulting in a final surface area of 2.7 m²/g, which was determined by Brunauer–Emmett–Teller (BET) technique.

The foaming suspension contained LSCF particles dispersed in ink vehicle (Johnson Matthey 62/3 medium) with the polymer precursor solution. The prime component of the ink was terpineol and ethyl cellulose (with a viscosity ~10,000 cP at room temperature at 10 s). The polyurethane (PU) precursor components were premixed into the ink vehicle before the incorporation of the LSCF particles. The initial PU precursor consisted of polymethylene polyphenyl isocyanate (Mn $\sim$ 340; Sigma-Aldrich, St. Louis, MO) and polyethylene glycol (PEG200; Sigma-Aldrich) with polyoxyethylene sorbitan monooleate (Tween 80; Fluka Chemie GmbH, Buchs, Switzerland).[2,4] Exposure of the foaming suspension to a reagent (water) initiated the polymerization reaction, which produced carbon dioxide (CO_2) gas. The foamed structure obtained was destabilized due to Ostwald ripening and coalescence. To stabilize the structure, the Tween 80 surfactant was required.[2,4] The polymer precursors were premixed in various volumetric ratios within an argon-filled glove box (<0.1% relative humidity). The PU precursor system was then mixed with the cathode material in an appropriate volume ratio pertaining to the desired solids loading. The samples were exposed to the ambient atmosphere (45–55% relative humidity) in order to dry. The foamed samples were burned out at a rate of 1°C/min to 600°C and then sintered at a rate of 3°C/min to the determined sintering temperature for 2 h.

Similar LSCF architectures were direct foamed onto electrolyte-support membranes for electrochemical testing. The electrolyte membranes were fabricated from 8 mol% YSZ powder (Daiichi Kigenso Kagaku Kogoyo, Osaka, Japan) by a tape casting, lamination, and sintering process (~110 μm final thickness). A < 1 μm thick $Ce_{0.9}Gd_{0.1}O_2$ (GDC) buffer layer was incorporated between the electrolyte and both electrodes by screen printing and firing onto the electrolyte at 1350°C for 1 h. A 50 vol% LSCF-50 vol% GDC composite was formed as an active cathode composition and was printed as an ink on both sides of the electrolyte membrane (~5 μm thickness). For the baseline samples, a pure LSCF ink was printed over the active area and sintered to 1150°C for 1 h without foaming. The alternative cathode architecture was fabricated by printing a LSCF ink containing the polyurethane precursors. The ink was composed of LSCF powder (from the same powder lot) and the 8:4:1 polymer precursor composition (isoscyanate: polyol: surfactant). These materials were printed over the active layer within an argon-filled glove box. On exposure to ambient atmosphere (relative humidity 45–55%), the polymerization reaction was initiated, and the CO_2-blowing reaction resulted in the foaming of the printed LSCF structure. The LSCF/polymer thick film gel was then fired at 1150°C for 1 h. EIS was performed on the symmetrical cells where the LSCF thick films were deposited on each side of a YSZ electrolyte membrane. Using a Solartron SI-1287 potentiostat interfaced with a SI-1260 impedance analyzer, the EIS spectra were collected on the cathode architectures foamed with the different processing variables. The EIS was conducted at 750 and 800°C under different loading

conditions such as OCV, 100 mA, and 300 mA. The analysis and curve fitting of the data were then carried out using ZView® software (Scribner Associates, Southern Pines, NC). The EIS was performed under 50 sccm of ambient air at standard atmospheric pressure.

Quantitative analysis of the foamed LSCF pore microstructure is critical to correlate the processing parameters with the electrochemical performance.[8] Pore size distribution is commonly characterized through methods such as gas adsorption and/or mercury porosimetry, where the pore size is estimated from gas condensation or liquid wetting, respectively, where the pore sizes are derived from the capillary features of the pore channels (with various average radial sizes). These techniques provide a pore size distribution for the microstructure, but the data are still quite qualitative (with many theoretical assumptions) and the characterization provides little additional microstructural information related to the orientation, shape, and tortuosity of the pores. Regardless, the current work was initiated by utilizing these two techniques in an attempt to evaluate the average pore size and distribution for the foamed samples. The initial gas absorption work (using a Micromeritics ASAP 2020 unit with N_2 absorptive gas, Micromeritics Instrument, Norcross, GA) on the foamed films was only able to measure porosity characteristics <50 nm using Barrett–Joyner–Halenda (BJH) analysis. A foamed cathode specimen with 50 vol% LSCF powder in the ceramic–polymer precursor suspension using a stoichiometric precursor composition of 8:4:1 (precursor: PEG 200: surfactant) was initially fabricated and fired to 1150°C for 1 h. The gas absorption data indicated an average pore size of only 39.6 nm, which is not characteristic of the microstructure in this work using micrometer size LSCF powder. The same sample underwent mercury porosimetry using a Micromeritics Autopore IV 9500 porosimeter. The measurement indicated a more reasonable average pore size of 3.4 μm for the film, but the average porosity level was measured to be nearly 76.7%, which is far greater than the expected value (which will be later discussed). The error is aligned with the relatively small sample size of the bulk and thick film samples, where most mercury porosimetry instruments require at least a 25% stem film volume (as recommended by the manufacturers). In addition, further error will be introduced when the film is supported on a substrate, such as a cathode thick film on a dense electrolyte membrane. Due to these initial characterization issues encountered at the beginning of the work, an alternative method was required to provide quantitative information related to the pores size and distribution of the thick film samples. In addition, a characterization method that would
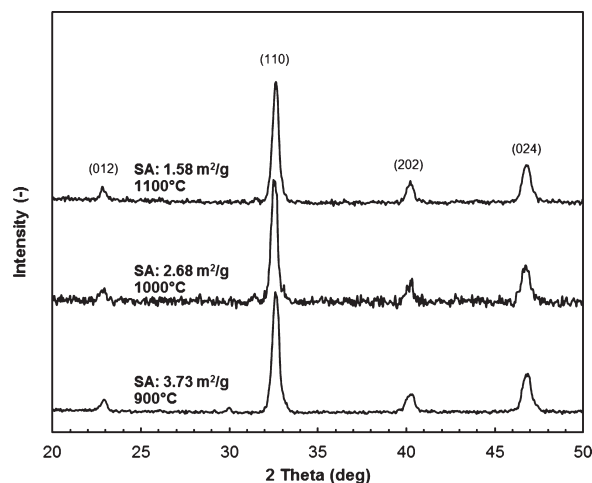

Fig. 1. XRD and measured surface area (SA) of the LSCF powder calcined at 900, 1000, and 1100° C for 4 h.
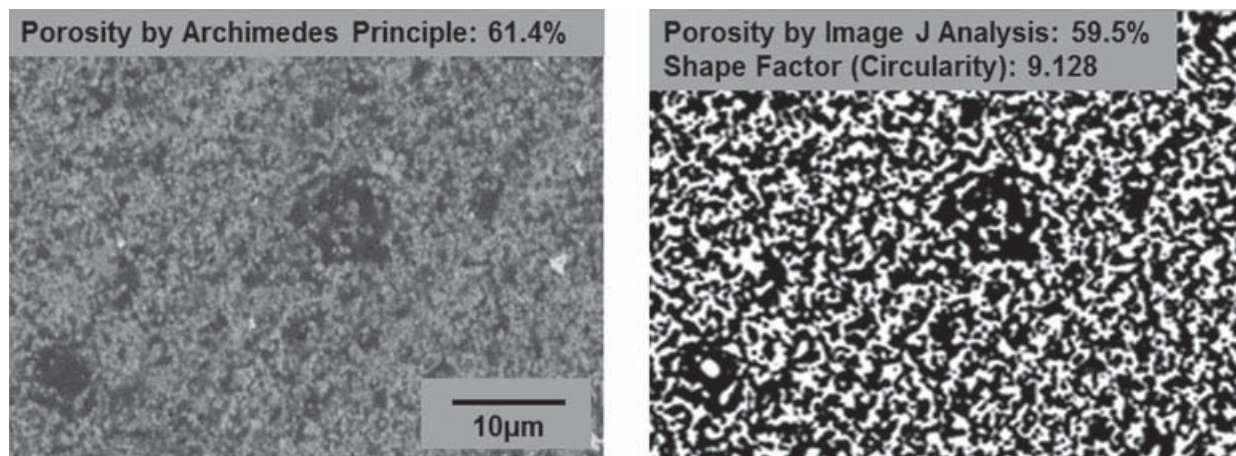
Fig. 2.   *Backscattered SEM image of a foamed LSCF sample (left), and the binarized version of the same picture used for computational image analysis (right).*

present more information regarding the pore geometry, orientation, and tortuosity was also desired.

To address the above-mentioned issues, the current work focused upon the use of stereological analysis to characterize the microstructure of the bulk and thick film LSCF foamed structures. The sintered cathode microstructures were mounted for the cross-sectioned imaging in a low-viscosity epoxy mixture (Allied Hitech Products, Rancho Dominguez, CA) with a weight ratio of 100:12 (epoxy resin: hardener). Air bubbles from this slurry were removed by vacuum, and the samples were later cured at room temperature for 8 h. The epoxy mounts were then polished down with 1 μm diamond paste. Scanning electron microscopy (SEM) was completed on the cross-sectioned samples using a JEOL 7600 SEM with backscatter imaging. Every sample was imaged at three different locations under three different magnifications (500×, 1000× and 2000×). Each data point represented herein is an average of 9 data points (images) per sample.

Typical line-intercept methods can be used for the quantitative analysis of the microstructure, which yields information related to grain/pore size and volume fractions.[8,9]

In this work, computer-assisted stereological analysis was completed on the 2D backscattered SEM images to obtain quantitative factors that describe the pore characteristics. The generally used parameters to quantify the microstructural properties are length maximum and minimum chords (d_{max} and d_{min}), perimeter (p), and surface area (A) of a pore or grain.[10–15] ImageJ (openware by the US National Institute of Health, Bethesda, MD) was used in this work to calculate these parameters with the

assistance of a customized java plug-in. Impoco[14] reported a software plug-in for ImageJ to analyze the SEM images of intricate and interconnected porous microstructures of cheese, which is similar to the microstructures of foamed cathode that are obtained through *in situ* foaming. This plug-in was adopted and modified to analyze the foamed cathode microstructures in this work. As shown in Fig. 2, the change in contrast and brightness, along with binarizing of the image, assisted in clearly distinguish between different phases in the micrograph. Mean pore area, form factors, porosity, pore aspect ratio, pore maximum and minimum diameter were all calculated through the analysis. The porosity levels (and other microstructure characteristics) are highly dependent upon the levels of contrast and brightness determined by the user. To correlate these levels with the actual microstructure, the porosity of the samples was measured by Archimedes method. The contrast and brightness levels were then continuously adjusted until the porosity levels measured by stereology matched that of the actual average porosity level measured by Archimedes method.

A unique shape factor was required to define the magnitude of tortuosity (estimated from the 2D images) for the foamed microstructures. This is especially important, as these microstructures display such a wide pore size distribution and highly interconnected porosity, where the estimation of an average pore size distribution is quite complex and unrepresentative of the microstructure. A circularity factor was defined in this work to represent this shape factor, with the circularity factor defined as the ratio of the mean perimeter of the pore to the mean Ferret's diameter (as shown in Fig. 3). As the
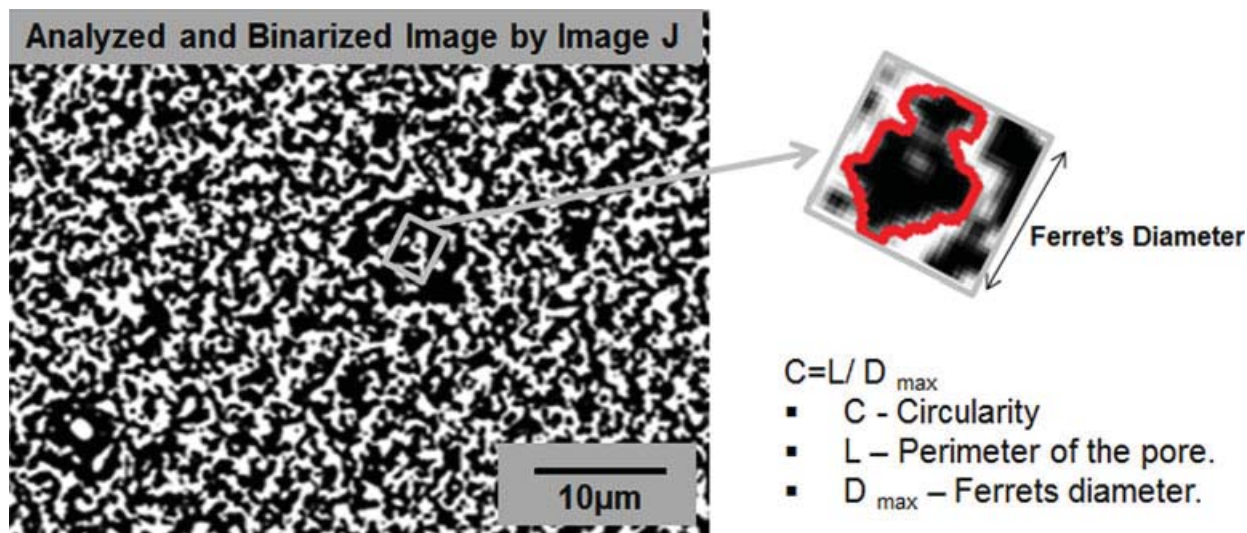
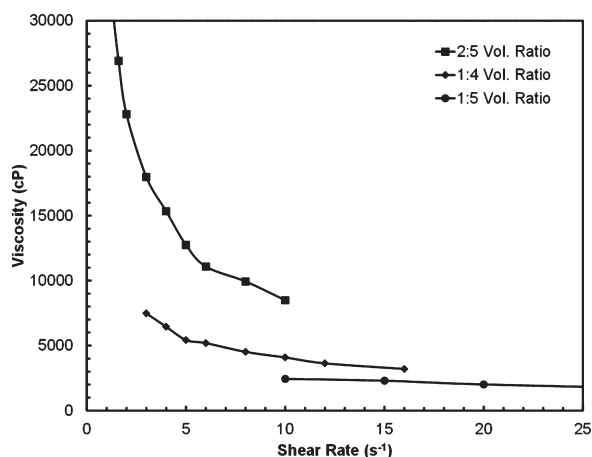Fig. 3. *Schematic demonstrating the method used to derive the circularity factor from the SEM images.*

Fig. 4. *Rheology measurements for the LSCF inks with different volume ratios of LSCF powder to ink vehicle (with no PU additives).*
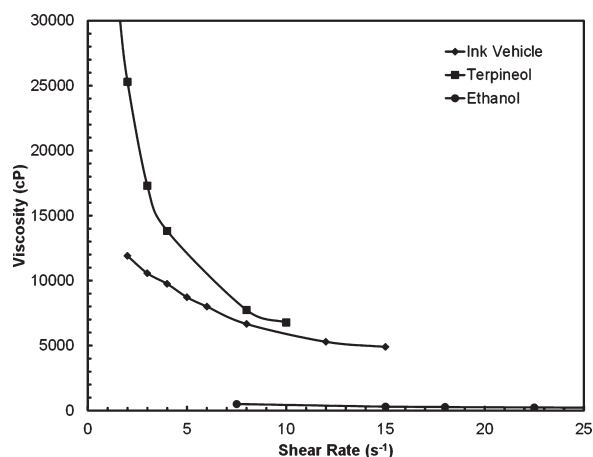
Fig. 5. *Rheology measurements of LSCF with the PU precursor mixture (8:4:1 ratio) using different solvents at a constant 2:5 vol ratio of solids to organic additive (solvent, terpineol, or ink vehicle).*

factor approaches the value of π (3.14), then the pore shape is more circular. The farther the value of the factor is from π, then the closer the pore is to an elongated or interconnected channel.

Results and Discussion

Effect of Solids Loading and Monomer Selection on Shear Thinning

The relationship of the solids loading and monomer content (before reaction) to the viscosity was evaluated. The initial experiments studied the viscous behavior of the LSCF particulate suspension within the terpineol/cellulose-based ink vehicle (with no polymer precursors). The LSCF powder was mixed thoroughly (by sonication) within the ink vehicle at LSCF/vehicle ratios of 1:5 (45–55 wt%), 1:4 (50–50 wt%), and 2:5 (62.5–37.5 wt%). Figure 4 displays the viscosity mapped against the shear rate, which shows that all the compositions exhibited shear thinning behavior (decrease in viscosity with the increase in shear rate).[16] A volume ratio of 2:5 for LSCF powder to ink vehicle displayed a viscosity in the region of 8000–10,000 cP at a shear rate of 10 s. This behavior is similar to that of commercially available LSCF inks with solids loading of 62–72 wt% and viscosity range of
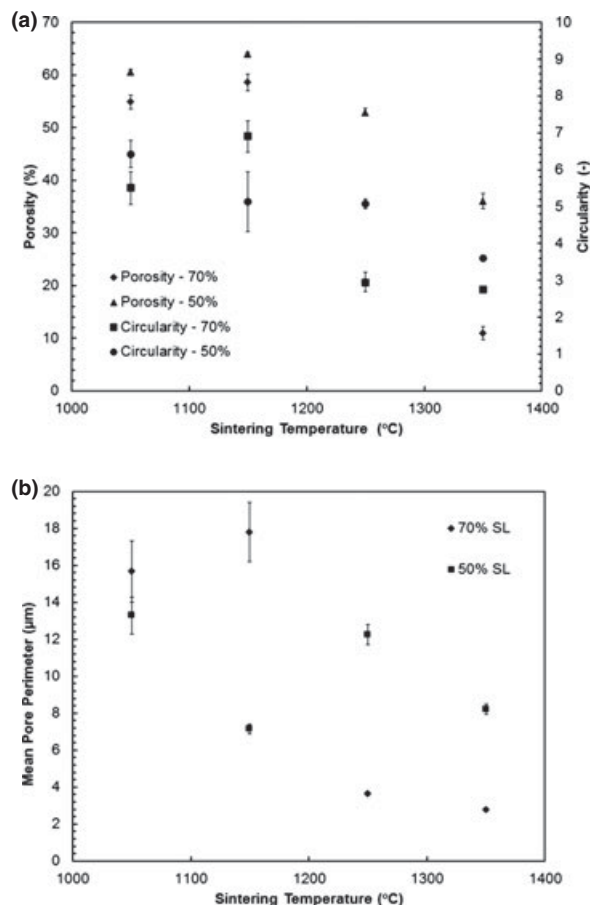
Fig. 6. (a) Average pore percentage and pore circularity and (b) mean pore perimeter as a function of solids loading for the LSCF cathodes foamed with 70% and 50% solids loading at 8:4:1 polymer precursor composition sintered between 1050 and 1350° C.

15,000–40,000 cP at a shear rate of 10 s. Greater viscosities were observed (at all shear rates) for solids loading compositions greater than 2:5. During cell fabrication, shear thinning behavior is desirable for retention of the printed design on the support after the shear force is released; in addition, the increased viscosity may assist encapsulation of evolved CO_2 gas during drying. The polymer precursors were then incorporated into the vehicle while maintaining the LSCF/vehicle ratio of 2:5. The polymer precursor composition included a common aromatic polymethylene polyphenyl isocyanate, PEG 200, and surfactant. The volume ratio of these components was maintained at the stoichiometric ratio of 8:4:1. The rheology measurement was completed without the presence of water or humidity. The samples displayed a similar shear thinning behavior with a viscosity ~6000 cP at 10 s, which is well within a desired screen printing processing range (Fig. 5).

Effect of Sintering Temperature on the Foamed Microstructure

LSCF cathode samples were foamed with two different solids loadings (50 and 70 vol%) at a constant stoichiometric polymer precursor composition. Samples at each solids loading were later sintered at temperatures of 1050, 1150, 1250, and 1350°C for 2 h. The image analysis study as shown in Fig. 6a displays the porosity, circularity factor, and mean pore perimeter plotted against sintering temperature. It shows that at both solids loadings, a significant fall in porosity and mean pore perimeter was observed at 1250 and 1350°C when compared with those of at 1050 and 1150°C. Circularity factor values closer to 3.14 indicate the collapse of the interconnected porosity and a tendency toward discrete circular pores. Above 1250°C, intensified densification of the foamed cathode was evident which resulted in the collapse of the pore architecture. In further tests, the same cathode composition was deposited onto YSZ substrates. Adhesion tests demonstrated that cathodes foamed over electrolytes adhered better at 1150°C than 1050°C. Therefore, owing to the high level of porosity and interconnected character, 1150°C was determined suitable for the rest of the work. The backscattered SEM images of bulk foamed cathode with 70% solids loading and 8:4:1 polymer precursor composition sintered at 1350°C and 1050°C are shown in Fig. 6b, where densification of the cathode microstructure is obvious at 1350°C.

Effect of LSCF Solids Loading on the Sintered Foamed Microstructure

A set of experiments with different solids loading of LSCF powder (50, 55, 60, 65, and 70 vol% in the ceramic–polymer precursor suspension) was synthesized and foamed. The stoichiometric precursor composition of 8:4:1 (precursor: PEG 200: surfactant) was retained for all solids loadings. Figure 7a displays a plot of the average porosity percentage and pore circularity as a function of solids loading for LSCF cathodes foamed with this polymer precursor composition and sintered at 1150°C. The specimens possessed a higher percentage of elongated or interconnected channels at higher solids loading. The data showed no significant change between 60% and 70% solids loading. An expected decrease in porosity is observed with an increase in solids loading, although the extent of this decrease was rather low. A decrease of ~10% was observed from the 50 vol% to 70 vol% solids loading with a level of 58% porosity at the 70 vol% solids loading.
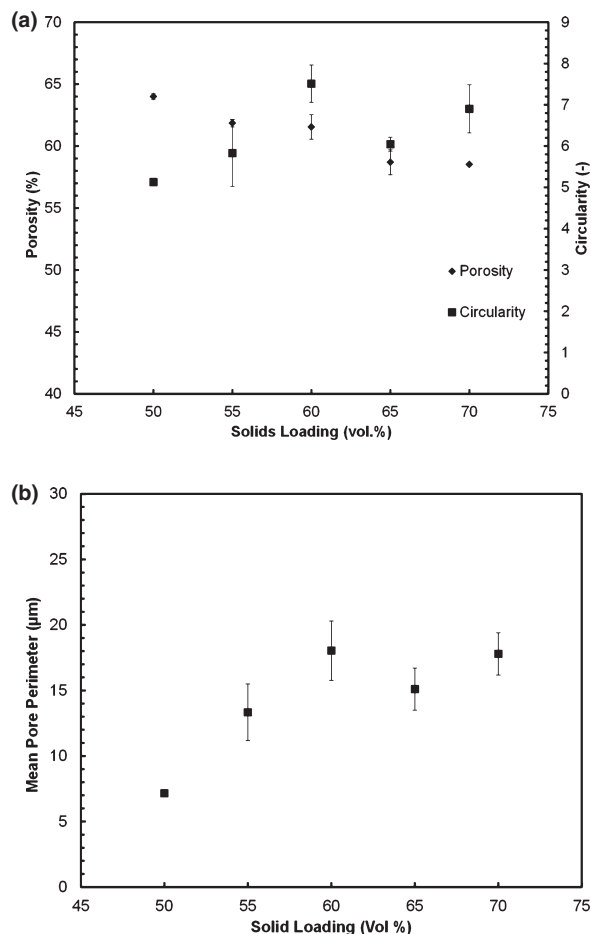
Fig. 7. *(a) Average pore percentage and pore circularity and (b) mean pore perimeter as a function of solids loading for the LSCF cathodes foamed with a 8:4:1 polymer precursor composition and sintered 1150° C.*

Fig. 8. *Backscattered SEM image of the foamed LSCF cathode with a 8:4:1 polymer precursor composition at 30 and 70% solids loading and sintered at 1150° C.*

Figure 7b displays a plot of the mean perimeter as a function of solids loading for LSCF cathodes foamed with a 8:4:1 polymer precursor composition and sintered at 1150°C. The perimeter (measured in the 2D projection) is a general indication of the level of surface area available for oxygen interaction and electrocatalytic reaction, where the second dimension is normalized into the plane of the micrograph. An appreciable rise in the mean perimeter observed with an increase in solids loading, and the highest mean perimeter of nearly 18 μm is observed at 70 vol% solids loading. This increasing trend of mean perimeter with solids loading is related to both the low buoyancy effect in densely packed material and the higher level of heterogeneous bubble nucleation and coalescence. These two effects result in a finer size level of porosity and increased overall mean perimeter. The high pore perimeter (measured in the 2D projection) is
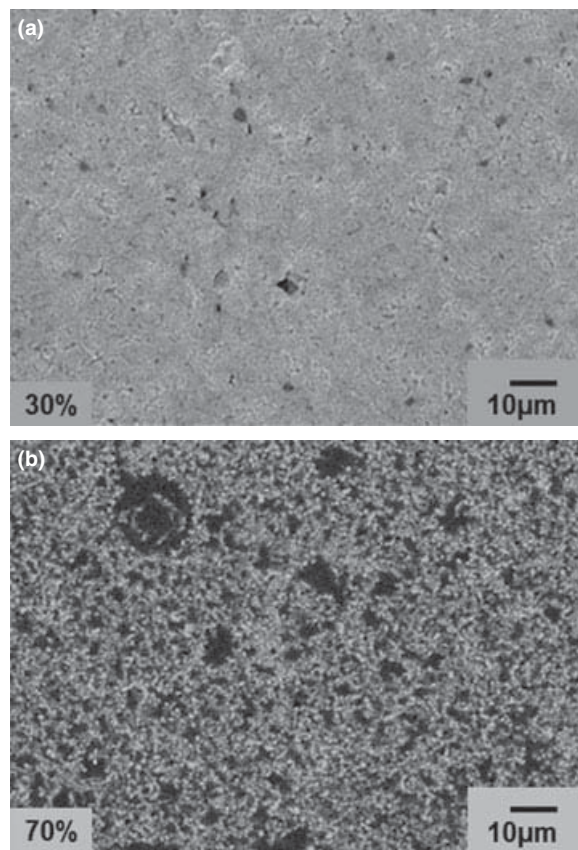
again a desirable feature in a SOFC cathode microstructure to maximize the surface area for gas–solid interaction and oxygen reduction reaction. Due to the mixed conduction capabilities of LSCF, this increased solid–gas area provides a larger total area for the oxygen reduction reaction and potentially increases the rate of oxygen incorporation into the electrolyte phase. The backscattered SEM images of the foamed cathode with 8:4:1 polymer precursor composition at 30 vol% and 70 vol% solids loadings and sintered at 1150°C are shown in Fig. 8.

Effect of monomer, polyol, and surfactant ratio on the sintered foamed microstructure

The following precursor compositions were evaluated with the isocyanate: polyol: surfactant volume ratios of 12:2:1, 8:6:2, 9:4:1, 8:4:1, and 8:4:2. A 70 vol% LSCF solids loading was used for all experiments with altered precursor compositions. The stoichiometric ratio
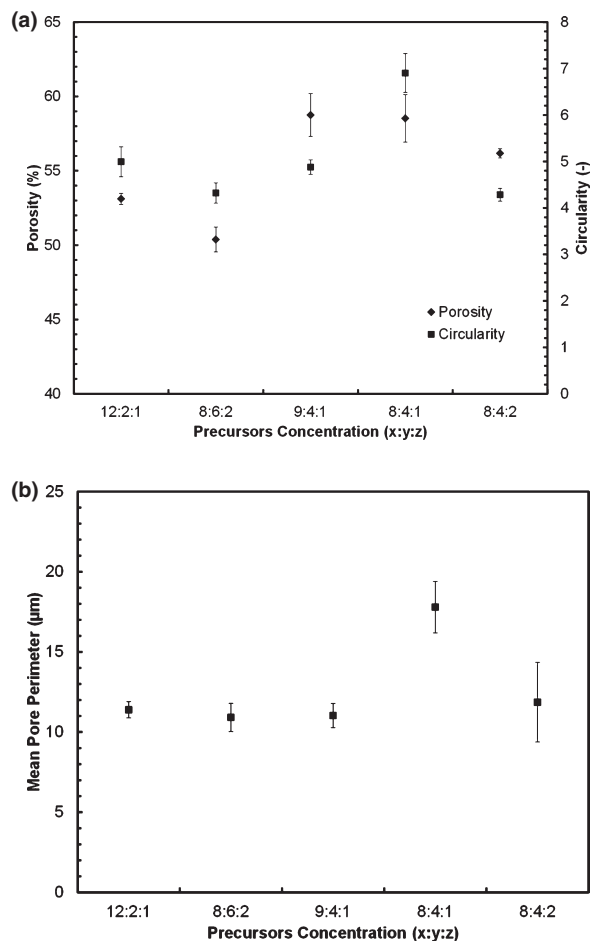
Fig. 9. (a) Percentage of average porosity and pore circularity and (b) mean perimeter (pore size) of the LSCF foamed microstructure as a function of polymer precursor composition. A 70% solids loading was utilized, and the final sintering for the foams was 1150°C.

of isocyante to hydroxyl groups for the polyurethane polymerization reaction is 2:1. The changes in microstructure were investigated by moving away from the stoichiometric ratio to account for both compositional within the solution.

Figures 9a and b display the plots showing the average porosity and pore circularity, and the mean pore perimeter, respectively, for the LSCF foamed microstructure as a function of polymer precursor composition. Figure 9a shows no significant change in the porosity level with a change in precursor ratio, and the average porosity remains within a 5% window. Interestingly, the pores formed with the stoichiometric polymer precursor composition of 8:4:1 (precursor: PEG 200: surfactant) exhibited a more tortuous geometry, where the circularity factor was found to be ~50% farther from π com-

pared with the other compositions tested. In addition, the same 8:4:1 ratio resulted in a higher mean pore perimeter compared with the other ratios (Fig. 9b). The mean perimeter for the stoichiometric composition was nearly 62% higher than those attained for the nonstoichiometric compositions 12:2:1, 8:6:2, and 9:4:1. The stoichiometric composition with the higher surfactant concentration (8:4:2) yielded pores with circularity factor (~4) much closer to π, which means that the pores were more circular and less interconnected. Also, the samples formed with this composition demonstrated a 51% reduction in the mean perimeter over those foamed with the 8:4:1. The surfactant was found to decrease the surface tension. The main purpose of the surfactant is to stabilize the foam by strengthening the cell windows and preventing coalescence or drainage effects, in addition to assisting bubble nucleation.[17–19] An increase in the surfactant concentration will increase the hydraulic resistance in the cell windows, resulting in over-stabilization and shrinkage of the foam.[20] The intrinsic pressure increase in the bubble cannot counter against the cell frame due to the higher surface tension, which yields smaller and less tortuous (more circular) pores. Hence, the 8:4:1 ratio previously demonstrated by a few other research groups [2,4] was found to be the most adequate polymer precursor composition for the production of a tortuous pore microstructure at a high particulate solids loading. Higher polyol additions result in structural features that would impart few benefits to oxygen reduction reaction processes.

Direct Foaming on a Dense YSZ Membrane Support

The electrochemical performance of the 8:4:2 and 9:4:1 foam precursor compositions was also examined by direct foaming the LSCF microstructures onto both sides of a YSZ electrolyte membrane. Within an argon-filled glove box, the LSCF ink containing the polymer precursor system was printed separately onto the active cathode layer which was symmetrically printed on both sides of the YSZ membrane. One major consideration in this process is that the typical free foam must not only densify during thermal processing, but must also bond to the substrate (and retain the microstructure previously described). The same foaming conditions were evaluated to investigate the processing–microstructure relationship when the ink was deposited on the electrolyte support. The final film thickness was approximately 60–70 μm. Figure 10 displays the backscattered SEM micrographs of a LSCF cathode cross section with a 8:4:1 polymer precursor composition (70% solids loading) foamed on the surface of a YSZ substrate and sintered at 1150°C.
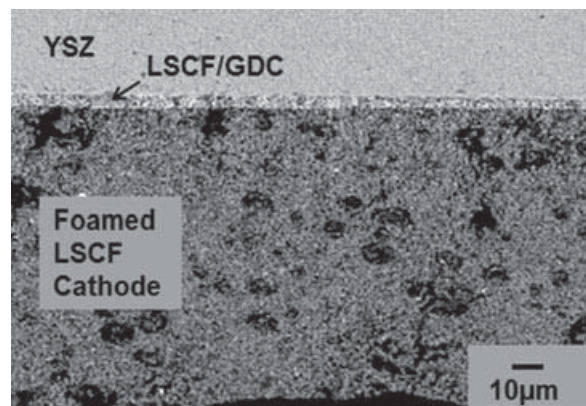
Fig. 10. Backscattered SEM micrograph of a LSCF cathode cross section with a 8:4:1 polymer precursor composition (70% solids loading) foamed on the surface of a YSZ substrate and sintered at 1150° C.
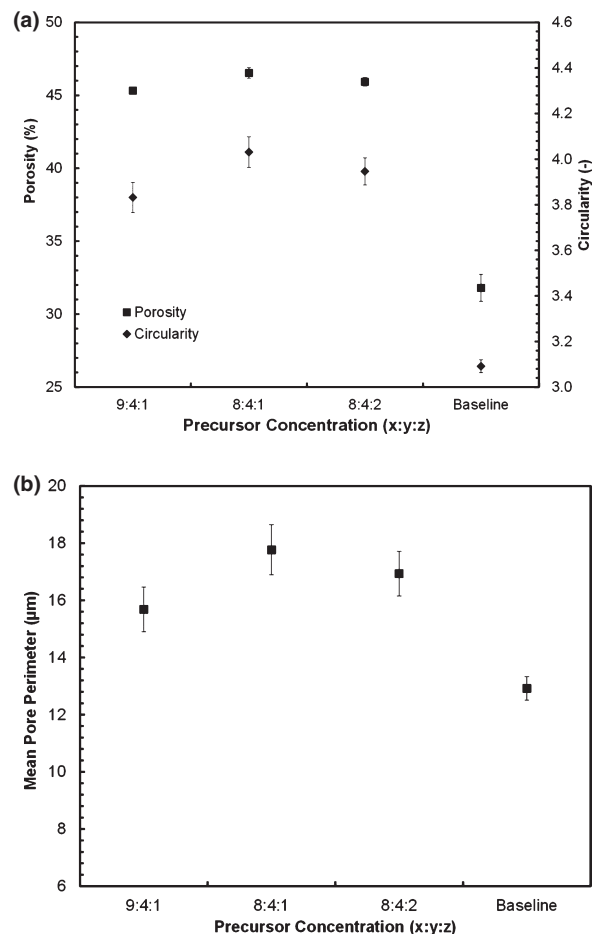

Fig. 11. (a) Percentage of average porosity and pore circularity and (b) mean perimeter of the LSCF foamed microstructure as a function of polymer precursor composition printed on a YSZ electrolyte support. A 70% solids loading was utilized, and the final sintering for the foams was 1150° C.

Figure 10 displays one side of the symmetrical cell, where the electrolyte, cathode active layer and foamed cathode layers can be identified.

Measured average porosity and circularity factors are shown in Fig 11 for the foamed cathode microstructure with the two precursor compositions sintered at 1150°C. The same figure shows the microstructural factors measured for samples where the LSCF powder was printed on the substrates without the use of foaming reagents and sintered at the same temperature. The results from the cathodes foamed over the YSZ substrates followed a trend similar to previous results observed for the bulk foamed cathode. The foamed microstructures displayed a high level of porosity (~46%) compared against the unfoamed samples (32%). In addition, the foamed microstructures showed a high circularity factor. The mean perimeters for the samples are shown in Fig. 11b, and the measured values were found to be 17.76 μm for the foamed cathode with a stoichiometric 8:4:1 composition (standard composition), which was 15%, 7%, and 37% higher than the 9:4:1, 8:4:2, and baseline compositions (15.6, 16, and 12.9 μm^2, respectively).

The two-dimensional mean pore areas of the three foamed compositions (compared against the unfoamed microstructure) were measured near the top surface and ~2–5 μm above the LSCF/GDC active layer for each sample. The data for the two positions for each sample are presented in Fig. 12. A noticeable difference in mean pore area is observed between the two locations. The pores at the top of the cathode (the region farthest from the substrate) display a higher mean pore area than the location near to the substrate, although the porosity level appears similar for the corresponding compositions;

8:4:1 (48%), 8:4:2, and 9:4:1 (46%). Differences may relate to the coalescence of the bubbles as they progress through the film thickness due to the buoyancy force. In addition, the initial nucleation kinetics of gas bubbles may be higher near the rough electrolyte surface when the solvent content is high (before complete drying), resulting in an initially higher concentration of the finer discrete pores. The circularity factor was maintained at the two locations. The slight increase in pore size farther from the electrolyte interface may assist in gas diffusion, while smaller pores near the electrolyte increase surface area for oxygen reduction. In addition, the population of large pores near the electrolyte should be minimized to maintain a bonding strength at the interface. Although a difference in the mean pore area was shown between the two locations, the magnitude of the gradient was low
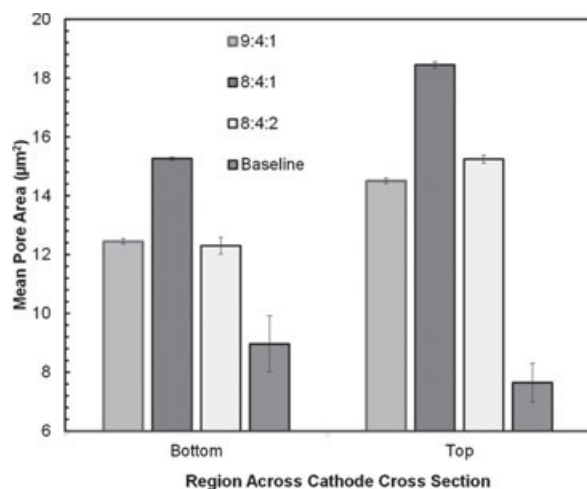
Fig. 12. Mean pore area as a function of location for LSCF films foamed with different polymer precursor compositions (and 70% solids loading) on a YSZ substrate and sintered at 1150°C.

(~25% difference) due to the minimal thickness of the film, which does not permit appreciable differences in the gas bubble nucleation and growth kinetics across the small distance.

Electrochemical Testing of the Foamed Cathode Microstructures

As discussed previously, the foamed cathode microstructures were printed symmetrically on both sides of the YSZ membranes (which included a GDC barrier and LSCF/GDC active layer on both sides), and these cells were tested by EIS at 750°C and 800°C at 0 mA, 100 mA, and 300 mA current loadings. The 9:4:1, 8:4:1, and 8:4:2 precursor compositions (monomer: PEG 200: surfactant), as well as the baseline (unfoamed) cathode, were all tested at these conditions. Figure 13 displays the electrochemical impedance spectra collected for all foamed compositions and the unfoamed cathode at 750°C and 800°C. The polarization curves were normalized to zero on the real axis by removing the ohmic resistance (high frequency contribution) due to the slight variations in the electrolyte thickness. The polarization resistance of the unfoamed cathode was measured to be 0.36 Ω cm^2 at 800°C under 0 mA current. This value is similar to that reported in literature for LSCF composite cathodes at 800°C under 0 mA current (0.45 Ω cm^2 [21] and 0.4 Ω cm^2 [22]). The total polarization for the entire symmetrical cell with a foamed cathode displayed a combined electrode polarization of 0.16 Ω cm^2 (thus, a singular cathode polarization of 0.08Ω cm^2) at 800°C. Polarization of the foamed sample with 8:4:1 precursor

composition was lower at 100 mA and 300 mA current at both temperatures when compared with other compositions. The 9:4:1 and 8:4:2 compositions displayed polarization similar to the baseline at 800°C, with values of 0.4 Ω cm^2 (9:4:1), 0.38 Ω cm^2 (8:4:2), and 0.36 Ω cm^2 (unfoamed) at 0 mA, 100 mA, and 300 mA, respectively. The peak point of the impedance curves for all the compositions and at both temperatures was observed at and near 100 Hz. It indicates that the charge-transfer resistance is acting as the limiting mechanism against the oxygen reduction reaction in the cathode.[23,24] A decrease in peak point value for the cell with 8:4:1 composition compared with others at same 100 Hz can be seen in Fig. 13. This explains the effectiveness of microstructures with wide pore size distribution and elongated pores in mitigating the charge-transfer resistance and consequently enhancing ORR.

Conclusion

An *in situ* direct foaming process was investigated for the first time to form a porous LSCF thick film microstructure for SOFC cathode applications. The foaming process was based upon the use of the gelling and blowing reactions resulting from the polyurethane polymerization. The study characterized the foamed microstructure resulting from monomer selection, organic precursor composition, LSCF solids loading, and sintering temperature. Green processing variables had significant effect on the gas bubble nucleation and growth governing forces, which resulted in appreciable changes to pore size, shape, and interconnection. The quantitative analysis of the microstructural characteristics was completed through 2D stereological image analysis of SEM micrographs, and correlations between the processing and microstructure were presented. This characterization method was chosen over typical gas absorption and porosimetry methods so that a consistent technique could be used to compare the microstructures of both the bulk and the thick film samples. In addition, the stereological image analysis provided additional information regarding the porosity shape and tortuosity of the microstructure, which are not available using gas absorption and porosimetry techniques. Optimal strength and porosity for the microstructure were obtained in a foamed cathode processed in a terpineol-based ink vehicle with a solids to carrier vehicle ratio of 2:5 (solids: carrier vehicle), aromatic isocyanate monomer, and a solids loading of 70 vol%. A foamed cathode using a near stoichiometric polymer precursor composition (8:4:1) yielded a microstructure with a broad porosity level and
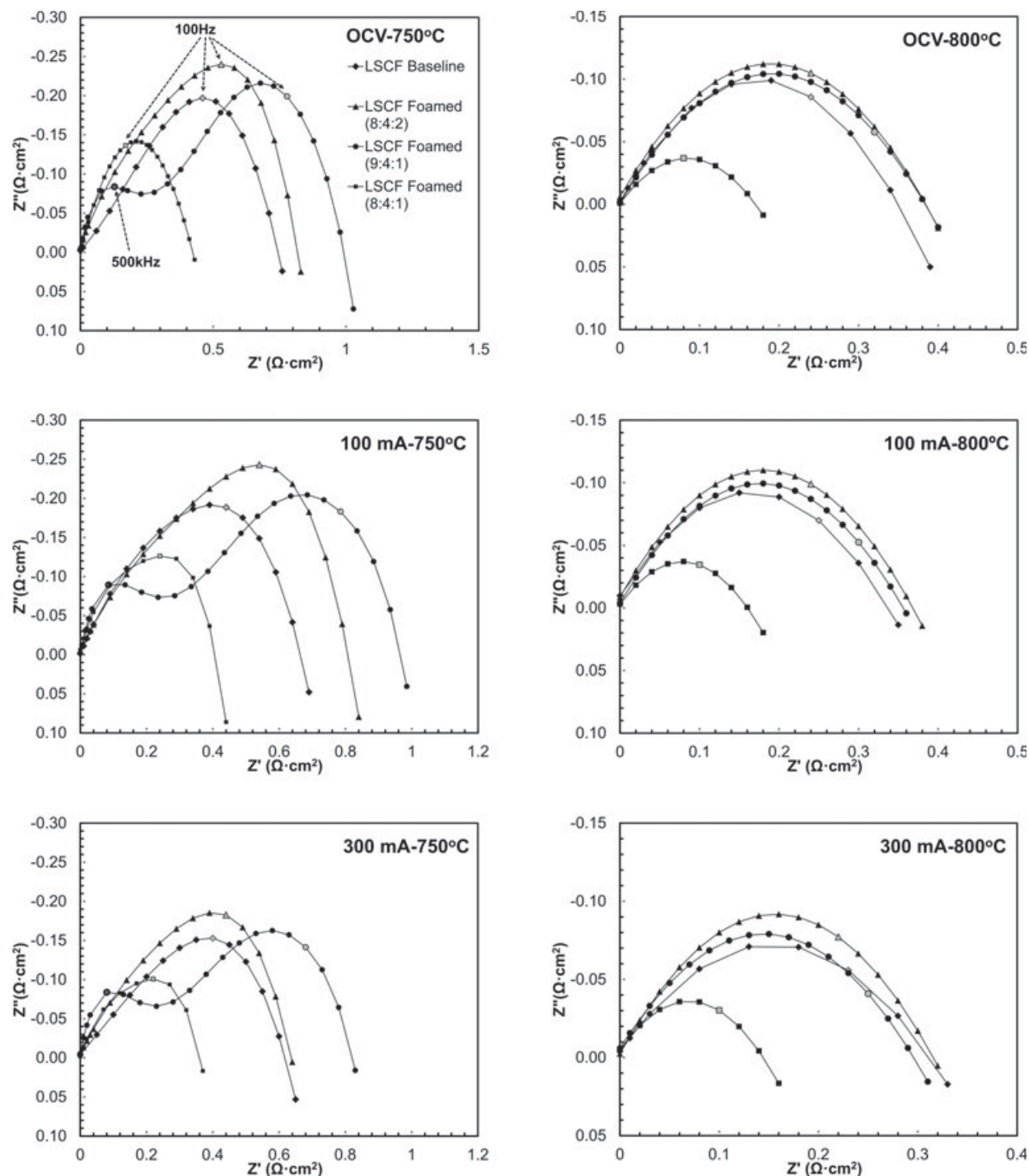
Fig. 13.   Electrochemical impedance spectroscopy (EIS) curves for symmetrical cells with foamed and unfoamed LSCF cathodes tested at 750° C (left) and 800° C (right) at 0 mA, 100 mA, and 300 mA.

highly interconnected microstructure after sintering at 1150°C.

The same polymer precursor composition and solids loading were used to direct foam the LSCF cathode onto an YSZ electrolyte as a thick film cathode. The foamed cathode was successfully sintered/bonded to YSZ substrates to demonstrate potential practical SOFC application. The change in the polymer precursor compositions

was examined on the substrate, and the resultant microstructures were shown to be similar to those previous produced in the bulk foaming. The electrochemical performance of the *in situ* foamed cathode was investigated through EIS testing, and a 50% decrease in the polarization resistance was measured when compared with the unfoamed (baseline) samples. The microstructural analysis and electrochemical testing of these foamed thick films demonstrated the processing method and showed the potential for future microstructural design of the cathode structure (specifically for increased TPB population, pore distribution/gradient, oxygen mass flow, and nanocatalyst incorporation). The microstructural design of these architectures can potentially be achieved through control of the polyurethane precursor content and surfactant type.

References

1. A. R. Studart, U. T. Gonzenbach, E. Tervoort, and L. J. Gaukler, "Processing Routes to Macroporous Ceramics: A Review," *J. Am. Ceram. Soc.*, 89 [6] 1771–1789 (2006).

2. A. Rainer, F. Basoli, S. Licoccia, and E. Traversa, "Foaming of Filled Polyurethanes for Fabrication of Porous Anode Supports for Intermediate Temperature – Solid Oxide Fuel Cells," *J. Am. Ceram. Soc*, 89 [6] 1795–1800 (2006).

3. S. J. Powell and J. R. G. Evans, "The Structure of Ceramic Foams Prepared from Polyurethane-Ceramic Suspensions," *Mater. Manuf. Processes*, 10 [4] 757–771 (1995).

4. L. Wucherer, J. C. Nino, F. Basoli, and E. Traversa, "Synthesis and Characterization of $BaTiO_3$- Based Foams with a Controlled Microstructure," *Int. J. Appl. Ceram. Technol.*, 6 [6] 651–660 (2008).

5. Y. W. Lo, W. C. J. Wei, and C. H. Hsueh, "Low Thermal Conductivity of Porous Al_2O_3 Foams for SOFC Insulation," *Mater. Chem. Phys.*, 129 [1–2] 326–330 (2011).

6. L. W. Tai, M. M. Nasrallah, H. U. Anderson, D. M. Sparlin, and S. R. Sehlin, "Structure and Electrical Properties of $La_{1-x}Sr_xCo_{1-y}Fe_yO_3$. Part 2. The System $La_{1-x}Sr_xCo_{0.2}Fe_{0.8}O_2$," *Solid State Ionics*, 76, 273–283 (1995).

7. C. Sun, R. Hui, and J. Roller, "Cathode Materials for Solid Oxide Fuel Cells: A Review," *J. Solid State Electrochem.*, 14 [112] 5–1144 (2010).

8. K. R. Lee, S. H. Choi, J. Kim, H. W. Lee, and J. H. Lee, "Viable Image Analyzing Method to Characterize the Microstructure and the Properties of the Ni/YSZ Cermet Anode of SOFC," *J. Power Sources*, 140 [2] 226–234 (2005).

9. S.-M. Bae, H.-Y. Jung, and J. H. Lee, "Microstructural Characterization of Composite Electrode Materials in Solid Oxide Fuel Cells via Image Processing Analysis," *J. Korean Ceram. Soc.*, 47 [1] 86–91 (2010).

10. B. Z. Altunkaynak, Z. Berrin, M. E. Onger, M. E. Altunkaynak, E. Ayranci, and S. Canan. "A Brief Introduction to Stereology and Sampling Strategies: Basic Concepts of Stereology," *NeuroQuantology* 10 [1] 31–43 (2012).

11. T. J. McCabe, L. V. Godby, and J. R. Transorra, *Metallographic Sample Preparation Techniques and Image Analysis for Density Distribution Determination in Steel Powder Compacts*, Advances in Metallurgy and Particulate Vol. 2, Materials Metal Powder Industries Federation, Princeton, NJ, 1994.

12. T. Wejrzanowski, W. L. Spycharlski, K. Rozniatowski, and K. J. Kurzydlowski, "Image Based Analysis of Complex Microstructures of Engineering Materials," *Int. J. Appl. Math. Comp.*, 18 [1] 33–39 (2008).

13. M. Oberholzer, M. Ostreicher, H. Christen, and M. Bruhlmann, "Methods in Quantitative Image Analysis," *Histochem. Cell Biol.*, 105 [5] 333–355 (1996).

14. G. Impoco, "Software for the Image Analysis of Cheese Microstructure from SEM Imagery," Available at http://svg.dmi.unict.it/Corfilac/downfiles/SEM-Analysis.pdf (accessed March 10, 2011).

15. J. H. Lee, H. Moon, H. W. Lee, J. Kim, J. D. Kim, and K. H. Yoon, "Quantitative Analysis of Microstructure and its Related Electrical Property of SOFC Anode, Ni–YSZ Cermet," *Solid State Ionics*, 148 [15] 15–26 (2002).

16. D. Burnat, P. Ried, P. Holtappels, A. Heel, T. Graule, and D. Kata, "The Rheology of Stabilised Lanthanum Strontium Cobaltite Ferrite Nanopowders in Organic Medium Applicable as Screen Printed SOFC Cathode Layers," *Fuel Cells*, 10 [1] 156–165 (2010).

17. Y. C. Tu, "Polyurethane Foams from Novel Soy-based Polyols," PhD dissertation, University of Missouri, Columbia, MO, 2008.

18. P. Król, *Linear Polyurethanes: Synthesis Methods, Chemical Structures, Properties and Applications*, KoninKlijke Brill NV, Leiden, The Netherlands, 2008.

19. Dow Polyurethanes - Surfactants Role in Foam Formulations, The Dow Chemical Company, Available at https://dow-answer.custhelp.com/app/answers/detail/a_id/5709/~/dow-polyurethanes—surfactants-role-in-foam-formulations (accessed March 1, 2011).

20. P. Mondal and D. V. Khakhar, "Hydraulic Resistance of Rigid Polyurethane Foams. II. Effect of Variation of Surfactant, Water, and Nucleating Agent

Concentrations on Foam Structure and Properties," *J. Appl. Polym. Sci.*, 93 [6] 2830–2837 (2004).

21. J. W. Yun, J. Han, S. Pil Yoon, S. Park, H. S. Kim, and S. W. Namb, "$Ce_{0.8}Gd_{0.2}O_2$ modification on $La_{0.6}Sr_{0.4}Co_{0.2}Fe_{0.8}O_3$ Cathode for Improving a Cell Performance in Intermediate Temperature Solid Oxide Fuel Cells," *J. Ind. Eng. Chem.*, 17, 439–444 (2011).

22. A. Esquirol, N. P. Brandon, J. A. Kilner, and M. Mogensen, "Electrochemical Characterization of $La_{0.6}Sr_{0.4}Co_{0.2}Fe_{0.8}O_3$ Cathodes for Intermediate-Temperature SOFCs," *J. Electrochem. Soc.*, 151 [11] A1847–A1855 (2004).

23. S. Lee, N. Miller, and K. Gerdes, "Long-Term Stability of SOFC Composite Cathode Activated by Electrocatalyst Infiltration," *J. Electrochem. Soc.*, 159, F301–F308 (2012).

24. A. Leonide, V. Sonn, A. Weber, and E. Ivers-Tiffee, "Evaluation and Modeling of the Cell Resistance in Anode-Supported Solid Oxide Fuel Cells," *J. Electrochem. Soc.*, 155, B36–B41 (2008).